

## Article

# Study on the Dynamic Response of Offshore Triceratops under Freak Waves

Nagavinothini Ravichandran <sup>1</sup> and Butsawan Bidorn <sup>1,2,\*</sup><sup>1</sup> Center of Excellence in Interdisciplinary Research for Sustainable Development, Faculty of Engineering, Chulalongkorn University, Bangkok 10330, Thailand; vino.civil35@gmail.com<sup>2</sup> Department of Water Resources Engineering, Chulalongkorn University, Bangkok 10330, Thailand

\* Correspondence: butsawan.p@chula.ac.th

**Abstract:** Freak waves are characterized by extreme wave height, irregular wave shape, high peak energy, short duration, and formidable destructive potential, posing a significant threat to offshore structures. Therefore, analyzing dynamic responses exhibited by advanced offshore platforms such as the offshore triceratops under the influence of freak waves holds paramount importance. However, the response analysis of offshore triceratops under freak waves has not been explored so far in the literature. Hence, the present study aims to investigate the dynamics of offshore triceratops intended for ultradeep waters under the impact of freak waves. Initially, the dual superposition model was utilized to generate the freak waves, and the numerical model of the platform was developed using ANSYS AQWA. Subsequently, the dynamic response characteristics of offshore triceratops under the influence of freak waves were analyzed in the time domain. The results demonstrate the effects of freak waves on the surge, heave, and pitch responses of the deck and buoyant legs were substantial, leading to a significant increase in maximum responses and variations in mean shift and standard deviations. The innovative insights derived from this study can serve as a benchmark for validating the effective performance and design of offshore triceratops.

**Keywords:** dynamic response; freak waves; numerical analysis; offshore triceratops; tether tension



**Citation:** Ravichandran, N.; Bidorn, B. Study on the Dynamic Response of Offshore Triceratops under Freak Waves. *J. Mar. Sci. Eng.* **2024**, *12*, 1260. <https://doi.org/10.3390/jmse12081260>

Academic Editor: Muk Chen Ong

Received: 25 June 2024

Revised: 12 July 2024

Accepted: 22 July 2024

Published: 26 July 2024



**Copyright:** © 2024 by the authors. Licensee MDPI, Basel, Switzerland. This article is an open access article distributed under the terms and conditions of the Creative Commons Attribution (CC BY) license (<https://creativecommons.org/licenses/by/4.0/>).

## 1. Introduction

Freak waves, also known as rogue or monster waves, are waves with huge wave heights, extremely fast propagation speed, irregular wave shape, strong nonlinear characteristics, and unpredictable occurrence [1]. These waves represent one of the most dangerous waves in the domain of ocean engineering and have significantly larger wave heights compared with the surrounding sea states. They tend to have thin wave crests, concentrated energy, strong nonlinearity, asymmetry, and a broad-banded spectrum that may cause severe damage to marine structures [2]. The likelihood of encountering freak waves in the deep sea is high [3], and occasionally, freak waves are also accompanied by successive large waves occurring either before or after the peak wave, which pose an additional threat to the safety of offshore structures [4]. Significant hazards posed by the freak waves on oceanic structures include slamming, splashing, wave run-up, and overtopping.

The first insight into the phenomenon of freak waves was obtained in 1966 by Professor Laurence Draper through the analysis of wave height records from the National Institute of Oceanography [5]. The first freak wave was then recorded three decades later in January 1995, when the Draupner jacket platform in the North Sea was affected by the famous New Year wave. The wave measured 25.6 m from crest to trough, whereas the significant wave height of the surrounding sea state was only 11.92 m [6]. It was also reported that nearly 22 supercarriers have been lost after being confronted by freak waves from 1969 to 1994 [7]. An analysis of data recorded from 16 to 22 November, 1997 at North Alwyn has shown 21 freak waves [8]. Furthermore, the investigation carried out by the European project MaxWave in the heavy sea states and severe weather from the three weeks of satellite data

found a considerable number of freak waves with a maximum height of up to 25.0 m [9]. Recently, the research platform FINO-1, used to collect wind data in the North Sea, was severely damaged by a wave that reached a height of 18.0 m above mean sea level [10]. The probability of occurrence of freak waves is 1/3000 in standard irregular seas according to Rayleigh distribution [11]. However, the frequency of occurrence of freak waves has increased recently, as evidenced by global oceanographic observations [12]. It is important to note that the interaction between floating structures and freak waves is highly nonlinear and impulsive, which requires accurate and robust computational methodologies [1]. This emphasizes the need to consider the freak waves in the design phase of marine structures. Further, the accurate evaluation of the structural loading mechanism introduced by freak waves and the dynamic response of offshore structures against them is crucial for structural safety and hazard prevention.

Various studies have addressed the dynamic response of floating offshore structures to freak waves due to their significant impact on structural safety. Xu et al. (2024) examined the dynamic response of floating photovoltaic platforms and mooring line structures under simulated freak waves using the superposition approach, revealing significant surge motion response and tether tension variation [13]. Li et al. (2023) investigated the dynamic response of spar-type floating wind turbines under freak waves with different properties, using the improved phase modulation to simulate the freak waves, showcasing notable influences of freak wave parameters on structural performance [14]. Zeng et al. (2023) conducted an experimental investigation on the dynamic response of floating offshore wind turbines under various freak wave profiles, simulated by a modulation method by embedding freak wave profiles in Gaussian seas. The results reveal that the freak wave induced coupling effect on surge and pitch motions, which increased with the increase in freak wave height and period [15]. Furthermore, Zhong et al. (2023) reported the hydrodynamic characteristics of semisubmersible floating offshore wind turbines in freak waves using a coupled computational fluid dynamics and finite element mooring line model and found the dramatic surge motion of the platform and fairlead tension of the upstream mooring line [16]. Zeng et al. (2023) studied the dynamic response of floating offshore wind turbines under freak waves with a large crest and deep trough and observed the quadratic phase coupling on nacelle acceleration due to freak waves [17].

Moreover, Huo et al. (2023) investigated the wave-slamming characteristics of a typical floating wind turbine under freak waves by numerical simulations and experiments, where the freak waves were simulated using a combined wave-focusing model. The results demonstrate that the slamming pressure of a floating wind turbine under a freak wave is much larger than that under a conventional random wave with the same significant wave height [18]. Pan et al. (2023) conducted experimental studies on the hydrodynamic characteristics of submerged floating tunnels under freak waves and reported significantly larger motion responses induced by freak waves compared with random waves, far exceeding the proportion of corresponding wave height [12]. Huo et al. (2021) carried out experimental tests and numerical simulations to study the air gap response and wave-slamming loads of a semi-submersible offshore platform under a freak wave. The freak waves were modeled using the linear superposition method and the study identified the close association between freak waves and wave slamming [19]. Luo et al. (2020) investigated the freak wave impact on a tension-leg platform through wave flume experiments and reported violent motions of the platform caused by the high-crest freak wave [20]. Tang et al. (2016) reported the dynamic analysis of turret-moored FPSO systems in freak waves, highlighting the large dynamic response of the structure due to freak wave loads as a kind of impact load [21]. These studies collectively illustrate the complex interaction between the freak waves and various floating structures such as offshore semi-submersible platforms, TLPs, and FPSOs, providing key insight into their dynamic behavior. Further, the nonlinear effects induced by the focused wave groups on floating structures were also well documented in the literature [22–25]. This also underscores the need to assess the hydrodynamic response of recently developed offshore structural systems under freak waves to ensure their stability.

The offshore triceratops is one of the new-generation offshore-compliant platforms suitable for ultra-deep-water operations. Its innovative design features a deck connected to three floating buoyant legs via ball joints, which effectively restricts the transfer of rotational motions from the legs to the deck. This design minimizes the deck's response to rotational movements, ensuring safe operational conditions even in extreme ocean environments subjected to wind, waves, and current loads. The ball joints are pivotal in extending the operational capabilities of the offshore triceratops to ultradeep waters. Extensive studies were conducted to analyze the response of the platform under different sea states, including normal sea conditions with wind and wave loads [26–28], as well as extreme scenarios such as ice loads [29,30], earthquake loads [31], Arctic waters [32,33], and impact loads [33]. However, the specific dynamic behavior of the offshore triceratops under freak waves has not yet been documented in the literature. Ensuring adequate stability under diverse loading conditions is critical for offshore platforms to guarantee structural safety and optimal operability. Hence, to ensure the survivability of the offshore triceratops in harsh sea conditions, it is imperative to conduct a thorough assessment of the structure's ability to withstand freak waves.

In the scope of this investigation, the primary objective of the present study is to examine the response of offshore triceratops to freak waves. The freak wave is simulated as a focused group of waves derived from the JONSWAP spectrum using the dual superposition model. Subsequently, a numerical model of offshore triceratops for a water depth of 2400 m was developed in ANSYS AQWA solver. To validate the efficacy of the numerical model, preliminary free decay tests and motion responses under regular waves were conducted. Following this, a comprehensive time domain analysis was undertaken to ascertain the response of the deck, buoyant legs, and mooring lines of offshore triceratops under the influence of freak waves. A comparative evaluation of the platform's response under freak waves and its corresponding response under random waves was executed. The acquired insights into the effects of freak waves on this novel offshore platform offer a substantive basis for informed structural design considerations. It is noteworthy that this study represents a pioneering endeavor in exploring the dynamic response of offshore triceratops under the influence of freak waves.

The novel contribution of this study lies in its comprehensive numerical investigation of the dynamic response of offshore platforms to freak waves, coupled with a comparative analysis of responses under random waves. While prior research has examined the platform's dynamic response in varied sea states and extreme conditions, the specific dynamic behavior of the platform under freak waves remains unexplored in the existing literature. By simulating freak waves and analyzing the platform's response, this study seeks to bridge the gap and provide valuable insights to better understand the behavior of the deck, buoyant legs, and mooring system of the platform.

## 2. Materials and Methods

The methodology depicted in Figure 1 outlines the approach employed in this study. An initial step involved the development of a MATLAB program R2024a to simulate freak waves using the dual superposition method. The sea state parameters identified by Li et al. [14] as having a better freak wave simulation effect were taken into consideration for this study. Then, the numerical model of the offshore triceratops for ultradeep waters has been developed in ANSYS AQWA 2023 R2. Initially, free decay tests and simulations of the numerical model under standard operating sea conditions with regular waves were conducted to obtain the free decay curves and Response Amplitude Operators (RAOs). Subsequently, a time domain simulation was performed to analyze the dynamic characteristics of the offshore triceratops under the developed freak waves and the random waves. A comparison of the dynamic characteristics of the deck, buoyant legs, and tether tension was then carried out to establish the effects of freak waves on the structure.

This paper is structured as follows: Section 3 provides an overview of the simulation of freak waves to evaluate the structural response. In Section 4, the conceptual design of

offshore triceratops, numerical modeling, and free decay tests are introduced. Section 5 presents the findings of the time response analysis of offshore triceratops under freak waves, along with a comparison of responses under freak waves and random waves.

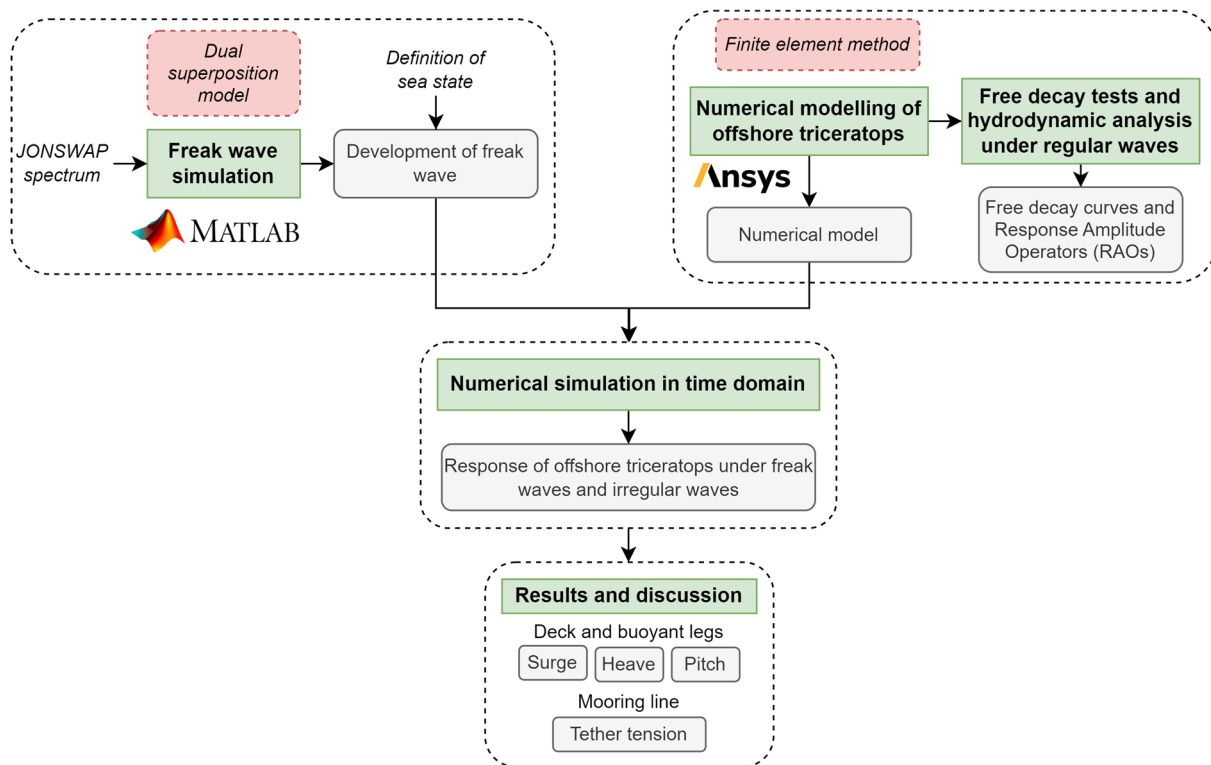


**Figure 1.** Methodology of this study.

### 3. Freak Wave Simulation

#### 3.1. Definition of Freak Wave

Freak waves are extreme environmental conditions that occur offshore, characterized by exceptionally high wave heights. They have been reported to cause significant damage and destruction to offshore structures over the past few decades [13]. While a precise definition of freak waves is yet to be established, their fundamental attributes can be delineated as follows: they represent the outermost end of the wave height probability distribution, they concentrate energy within a localized area, their emergence is sudden, and they pose greater hazards than the anticipated sea state [1]. The generation of freak waves and the prediction of their occurrence are continuously being explored due to their complexity and rarity. Field data have revealed that these waves can manifest under varied sea conditions, influenced by factors such as water depth, seabed topography, wind, and current patterns. Physical causes contributing to the occurrence of freak waves include dispersive environments, modulation instability, soliton collisions, atmospheric forcing, wave–current interactions, and geometric focusing [1]. Local environmental factors, such as seasonal changes in directional speed and high surface current velocity, may serve as early warning indicators for potential freak wave events [34]. The sudden accumulation of energy at the time of a freak wave occurrence is fundamental to their generation [35]. Given the distinctiveness of freak waves, it is imperative to precisely define their shape and the ratio between a freak wave and adjacent waves to avoid confusion with other extreme wave phenomena.

The formal definition of freak waves was first proposed by Klinting and Sand after analyzing a large amount of freak wave data [36]. The definition consists of three conditions summarizing the characteristics of freak waves and their relationship with the surrounding wave environment, as depicted in Figure 2. These conditions are currently the internation-

ally recognized definition of freak waves. These decision criteria are based on the heights of the previous wave (PW), freak wave (FW), and next wave (NW), within the time intervals of  $(t_1, t_2)$ ,  $(t_2, t_3)$ , and  $(t_3, t_4)$ , respectively.

- i. The ratio of the freak wave height to the significant wave height should be greater than two, i.e.,  $\alpha = H_j/H_s \geq 2$ , where  $H_j$  is the freak wave height, and  $H_s$  is the significant wave height.
- ii. The ratio of the wave crest height to the freak wave height should be greater than 0.65, i.e.,  $\mu = \eta_j/H_j \geq 0.65$ , where  $\eta_j$  is the freak wave crest (FWC) height.
- iii. The ratio of the freak wave height to the adjacent wave height should be greater than two, i.e.,  $\beta_1 = H_j/H_{j-1} \geq 2$ , and  $\beta_2 = H_j/H_{j+1} \geq 2$ .

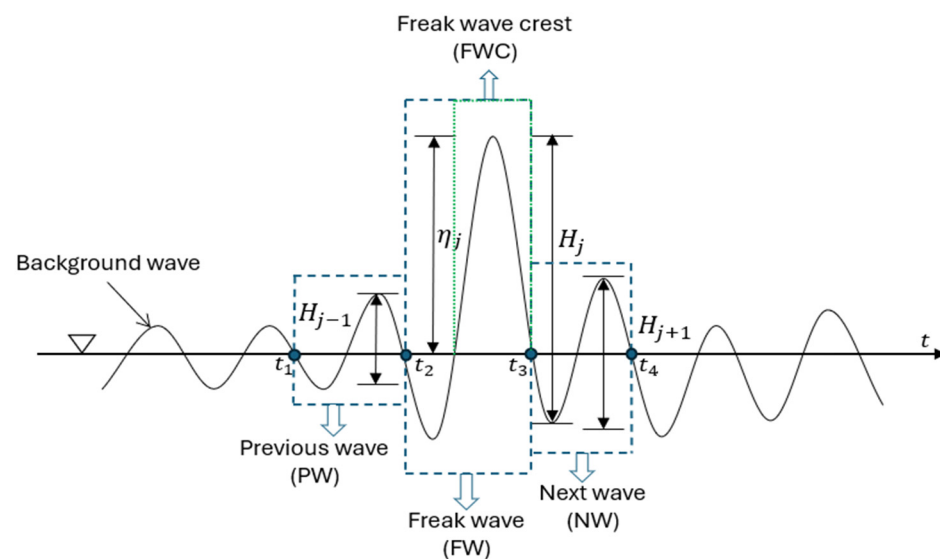


**Figure 2.** Representation of a typical freak wave.

### 3.2. Freak Wave Simulation

Extensive research has been conducted on the formulation mechanism of freak waves, yet simulating ideal freak waves through sophisticated approaches remains a challenge. Consequently, various methodologies have been devised for generating freak waves, broadly categorized as linear and nonlinear methods [1]. The Longuet-Higgins model (refer to Equation (1)) stands as a principal method for simulating freak waves. This linear superposition method is straightforward and efficient, resulting in stable waveforms. According to this theory, a unidirectional wave field can be viewed as a combination of waves with varying frequencies [37]:

$$\eta(x, t) = \sum_{i=1}^N A_i \cos(k_i x - \omega_i t + \varphi_i) \quad (1)$$

where  $\eta$  is the wave surface elevation,  $N$  is the total number of wave components,  $A$  is the wave amplitude,  $k$  is the wave number,  $\omega$  is the frequency of the individual wave, and  $\varphi$  is the random phase angle of an individual wave. For the simulation of the ordinary random wave, the phase angle is randomly chosen from a uniform distribution between 0 and  $2\pi$ . The wave amplitude can be obtained from the wave energy spectrum as follows:

$$\sum_{\omega_i}^{\omega_i + \Delta\omega_i} \frac{1}{2} A_i^2 = S(\omega_i) \Delta\omega_i \quad (2)$$

where  $\Delta\omega_i$  is the frequency interval between two adjacent wave frequencies, and  $S(\cdot)$  is the wave spectrum function. This linear wave theory is the basis for several methodologies developed for the generation of freak waves.

To model freak waves, it is necessary to concentrate the energy of specific wave components by adjusting the initial phase angle. A dual superposition model was employed for this purpose, as described in [38]. In this model, the total wave energy spectrum is divided into two parts: (i) background random wave,  $\eta_1(x, t)$ , and (ii) transient wave,  $\eta_2(x, t)$ , by assuming the occurrence of the freak wave at a time,  $t_c$ . The realization of the freak wave to the actual sea state was achieved by the first part of the wave elements. This approach allows the convergence of wave elevation to form an extreme wave at the focus position, meeting the freak wave decision criteria. Moreover, it facilitates simulating wave surface elevation to replicate the statistical characteristics of real sea conditions. Importantly, this method enables the generation of freak waves using only 15–20% of the total wave energy, indicating that a small portion of the overall wave energy can lead to the occurrence of a freak wave due to energy focusing. The wave elevation based on the dual superposition model is expressed as follows:

$$\eta(x, t) = \eta_1(x, t) + \eta_2(x, t) \quad (3)$$

$$\eta(x, t) = \sum_{m=1}^N A_{1m} \cos(k_m x - \omega_m t + \varphi_m) + \sum_{n=1}^N A_{2m} \cos(k_m(x - x_c) - \omega_m(t - t_c)) \quad (4)$$

where  $\varphi_m$  is the random phase angle varying from  $(0, 2\pi)$ ;  $x_c$  and  $t_c$  represent the distance and time of the occurrence of freak wave; and  $A_{1m}$  and  $A_{2m}$  are the amplitudes of the random and transient wave components expressed as follows:

$$A_{1m} = [2p_1 S(\omega) \Delta \omega]^{\frac{1}{2}} \quad (5)$$

$$A_{2m} = [2p_2 S(\omega) \Delta \omega]^{\frac{1}{2}} \quad (6)$$

where  $p_1$  and  $p_2$  are the proportions of the energy of the random and transient waves, respectively.  $p_1$  is equal to 80%, and  $p_2$  is equal to 20% [4]. The frequency spectrum is defined using the JONSWAP spectrum [39], which is a typical narrow-band spectrum, commonly used to generate freak waves [35]. It is expressed as follows:

$$S(\omega) = \frac{5}{16} H_s^2 \omega_p^2 \omega^{-5} \exp \left[ -\frac{5}{4} \left( \frac{\omega}{\omega_p} \right)^{-4} \right] (1 - 0.2587 \ln(\gamma)) \gamma^b \quad (7)$$

$$b = \exp \left[ -\frac{1}{2} \left( \frac{\omega - \omega_p}{\sigma \omega_p} \right)^2 \right] \quad (8)$$

$$\sigma = \begin{cases} 0.07, & \text{for } \omega \leq \omega_p \\ 0.09, & \text{for } \omega > \omega_p \end{cases} \quad (9)$$

where  $\omega_p$  is the peak frequency,  $H_s$  is the significant wave height, and  $\gamma$  is the peakedness parameter ( $\gamma = 3.3$  represents the standard sea spectrum). JONSWAP spectrum has the highest practical usage in ocean-related engineering studies, particularly on freak waves [16,17]. Further, studies on freak wave generation also highlighted the use of the JONSWAP spectrum due to the established result that developing storm dynamics are governed by this spectrum for a range of parameters [40,41].

The freak wave parameters reported to have a better freak wave simulation effect by Li et al. [14] have been chosen for the present study. The spectral parameters used in the simulation of freak waves are listed in Table 1. These parameters have the probability of generation of freak waves equal to 1.5% [14]. The random wave was generated from the JONSWAP spectrum with  $H_s = 6$  m and  $T_p = 10$  s, as shown in Figure 3.

The generated freak wave and the random wave are compared in Figure 4. The crest height of the simulated freak wave is 13.45 m, which is about 2.3 times larger than the random wave height of 6 m. Additionally, the time instances corresponding to PW, FW, and NW, as depicted in Figure 2, are  $t_1 = 581.4$  s,  $t_2 = 592.9$  s,  $t_3 = 601.7$  s, and  $t_4 = 613$  s. The FWC occurs within an interval of (598 s, 601.7 s), with the peak at 600 s. The peak frequency

of the simulated freak wave is 0.59 rad/s. Further, the generated freak wave parameters are as follows:  $\alpha = 3.31$ ,  $\mu = 0.69$ ,  $\beta_1 = 2.98$ ,  $\beta_2 = 2.21$ . These values can be seen fulfilling the conditions to confirm the characteristics of the freak wave according to its definition.

**Table 1.** Spectral parameters in simulating a freak wave.

Parameter	Value
Significant wave height, $H_s$	6 m
Peak period, $T_p$	10 s
Wave heading angle	$0^\circ$
Total simulated time, $t$	1000 s
Time step, $\Delta t$	0.1 s
FWC peak occurrence time, $t_c$	600 s
Frequency range, $\omega$	0.05–2
Peakedness parameter, $\gamma$	3.3

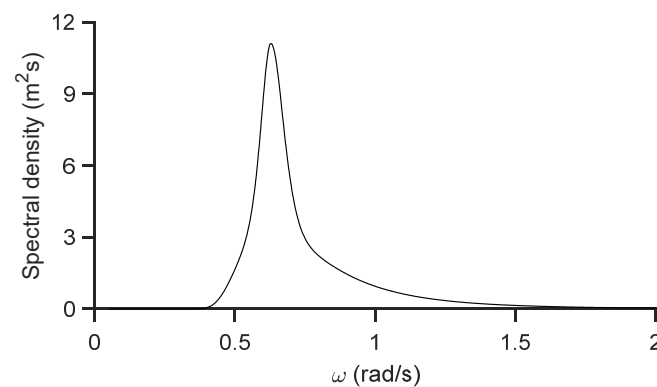


**Figure 3.** JONSWAP spectrum ( $H_s = 6$  m and  $T_p = 10$  s).

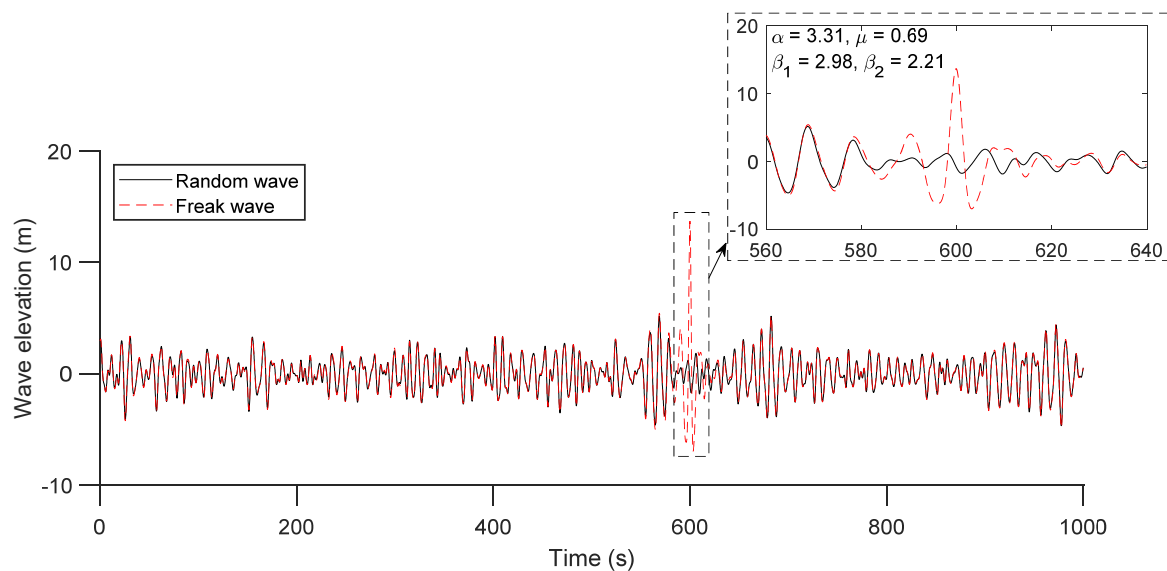


**Figure 4.** Comparison of random wave and freak wave ( $t_c = 600$  s).

## 4. Numerical Modeling of Offshore Triceratops

### 4.1. Offshore Triceratops for Ultradeep Waters

The offshore triceratops concept was initially proposed by Charles N. White in 2005 for ultra-deep-water depths ranging from 1500 m to 3000 m [42]. This innovative structural design comprises a deck, three buoyant legs (BL1, BL2, and BL3), ball joints, and tethers, as

depicted in Figure 5. The deck and buoyant legs are interconnected by ball joints, which transmit only translational motion while limiting rotational motion from the buoyant legs to the deck. This feature enhances the structural performance and operational conditions of the platform by minimizing deck rotation under extreme environmental circumstances. The buoyant leg units are deep-drafted cylindrical shell structures similar to the spar platform with excess buoyancy and are position-restrained by a set of taut moored tethers resembling tension leg platforms. The buoyant legs are typically designed as orthogonally stiffened cylindrical shells, deemed more suitable for offshore applications [43].

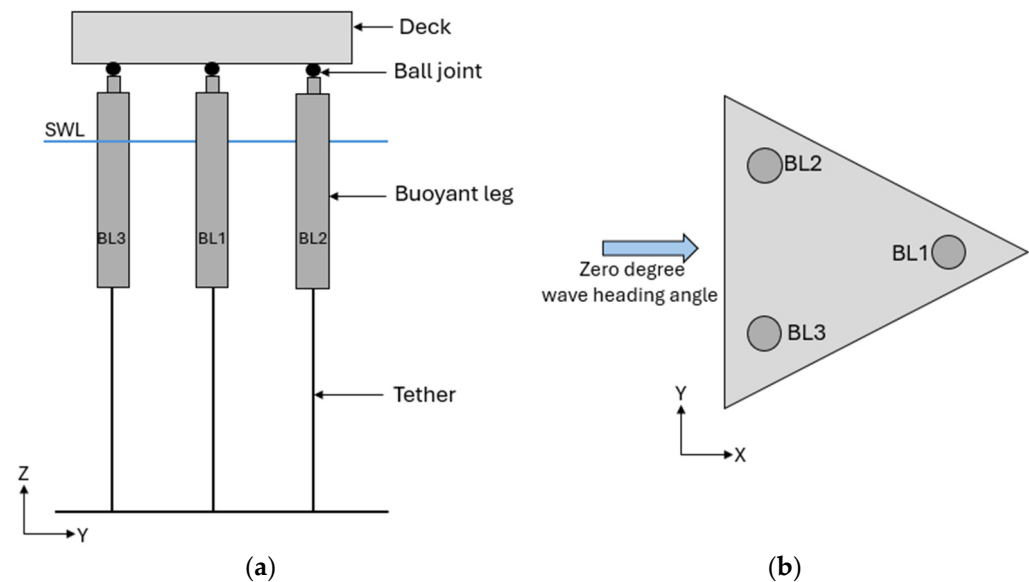


**Figure 5.** Conceptual model of offshore triceratops, (a) Front view, and (b) Top view.

In the present study, the offshore triceratops model, developed based on the dimensions of the Perdido spar in the Gulf of Mexico for a water depth of 2400 m, is being analyzed for its dynamic response under freak waves [26]. This particular structural design has demonstrated its suitability for ultradeep waters and extreme environmental conditions, attributed to its reduced deck response and strong recentering capability [26,27,29]. The main properties of offshore triceratops (deck and buoyant legs) and mooring systems are shown in Tables 2 and 3, respectively. The deck takes the form of an equilateral triangle with a length of 95 m, and the placement of the buoyant legs ensures stability by being positioned at an appropriate distance from the centroid. The platform's topside is engineered with three deck levels, forming an integrated truss deck system. Transverse tubular members stiffened with diagonal elements, are utilized to interconnect the various floor levels.

**Table 2.** Properties of offshore triceratops deck and buoyant legs.

Parameter	Value
Side length of deck	95 m
Distance between buoyant legs	61.70 m
Diameter of buoyant leg	15 m
Depth of buoyant legs below SWL	154 m
Depth of buoyant legs above SWL	20.24 m
Center of mass location below SWL	112.74 m
Metacentric height	35.83 m
Total weight (including payload)	$5.62 \times 10^8$ N
Buoyancy force	$8.21 \times 10^8$ N
Displacement	$2.72 \times 10^4$ m <sup>3</sup>
Principal second moment of inertia	$2.49 \times 10^3$ m <sup>4</sup>

**Table 3.** Parameters of the mooring system.

Parameter	Value
Tether length	2246 m
Tether diameter	1 m
Total tether force	$2.58 \times 10^8$ N
Stiffness of tethers	$2.20 \times 10^8$ N/m

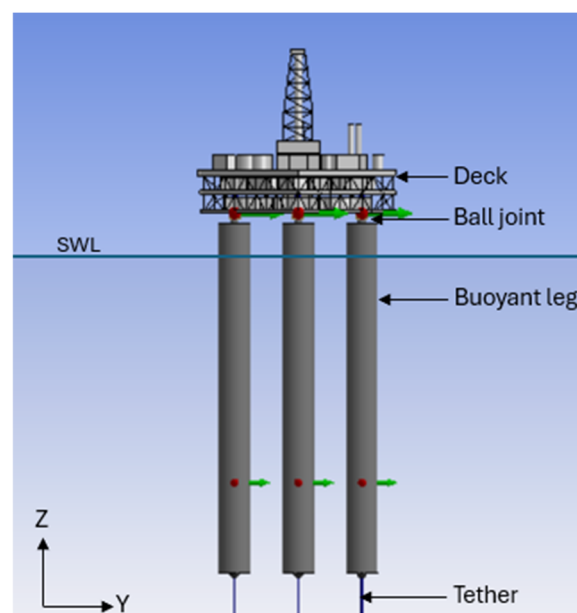
#### 4.2. Description of the Platform Model

The numerical model of the platform was developed using ANSYS AQWA 2023 R2 solver, where the buoyant legs were modeled as Morison elements. The legs were defined as TUBE elements in the solver, where the fluid force acting on the member is calculated using Morison's equation:

$$q_n = \frac{1}{2} \rho C_d d A (v_n - \dot{x}_n) |v_n - \dot{x}_n| + \rho d V a_n + (C_m - 1) \rho d V (a_n - \ddot{x}_n) \quad (10)$$

where  $\rho$  is the density of seawater,  $C_d$  is the drag coefficient,  $C_m$  is the inertia coefficient,  $dA$  and  $dV$  are the exposed area and displaced volume per unit length, respectively;  $v_n$  and  $a_n$  are water particle velocity and acceleration, respectively;  $\dot{x}_n$  and  $\ddot{x}_n$  are the velocity and the acceleration of the structure.

The structural integration of the buoyant legs involves ball joints linking to the deck on one side and taut-moored tethers securing the other side to the seabed. The tethers, modeled as linear cables with suitable stiffness and unstretched length to establish initial tension, play a critical role in the system. The meshing was conducted using a three-dimensional panel method, employing quadrilateral and triangular panels with a program-controlled optimal meshing approach, comprising 17,620 nodes and 17,198 elements. The deck weight and payload were applied at the mass center of the deck. Furthermore, the center of gravity, mass, and moment of inertia were specified as distinct inputs for both the deck and buoyant legs in the design modeler, contributing to the structural definition. The developed numerical model is shown in Figure 6.

**Figure 6.** Numerical model of offshore triceratops for ultradeep waters.

The simulation employed three-dimensional radiation theory to model the linearized hydrodynamic fluid wave loading. Hydrodynamic forces were computed using a three-point Gaussian integration scheme. Initially, a hydrostatic analysis was conducted on

the model, confirming the platform's stability with a positive metacentric height above the center of gravity. For time domain simulation, the real-time motion of the floating bodies was computed at each time step by integrating the accelerations in the time domain, utilizing a predictor-corrector numerical integration scheme. Finally, the dynamic response of the structure was obtained through time domain analysis under extreme and random wave conditions. The equation of motion which is solved by the convolution integration technique in ANSYS AQWA is given below:

$$[M + M_a] \ddot{x}(t) + [C] \dot{x}(t) + [K] x(t) = F(t) \quad (11)$$

where  $\ddot{x}(t)$ ,  $\dot{x}(t)$ ,  $x(t)$ , and  $F(t)$  are acceleration, velocity, displacement, and force vectors,  $M$  is the structural mass matrix,  $M_a$  is the added mass matrix,  $C$  is the damping matrix, and  $K$  is the stiffness matrix.

#### 4.3. Free Decay Tests and Response Amplitude Operators (RAOs)

Free decay tests were conducted in six degrees of freedom to determine the natural period and damping characteristics of the structure. During the test, the platform was released from an initial position away from its equilibrium state, with initial offsets of 10 m for surge, 2 m for heave, and  $2^\circ$  for pitch. The time-domain free decay response of the deck is illustrated in Figure 7. Damping was estimated using the logarithmic decrement method based on the free decay tests. The natural frequencies, and damping ratios obtained from the tests are presented in Table 4.

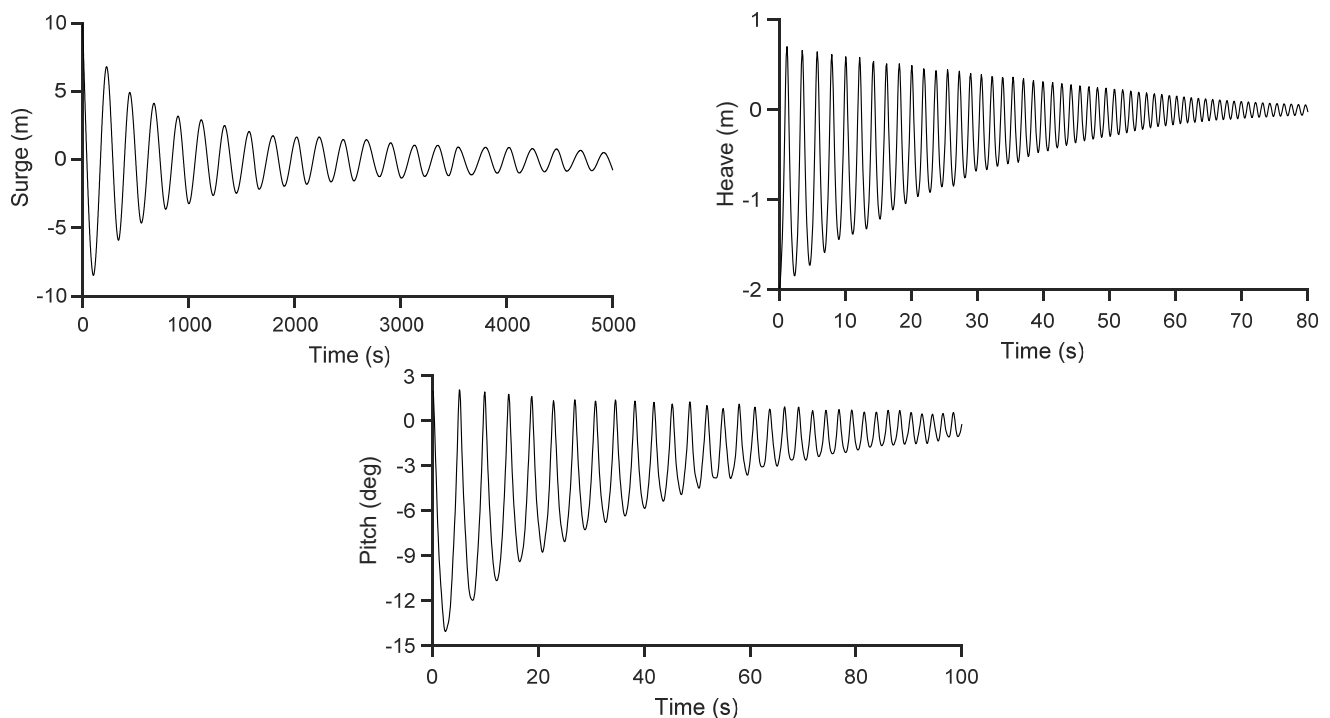


**Figure 7.** Free decay curves in surge, heave, and pitch degrees of freedom.

The free decay response of the deck was found to be symmetrical in the surge degree of freedom and unsymmetrical in the heave and pitch degrees of freedom. This can be attributed to the high initial pretension of the tethers. The low natural frequency in the surge direction highlights the high compliance of the platform in the horizontal plane. Conversely, the platform exhibits stiff motion in the vertical plane due to the taut moored tethers with high initial pretension, as evidenced by its high heave natural frequency. The surge and heave degrees of freedom show similar natural frequencies for the deck and buoyant legs, whereas a noticeable variation is observed in the pitch degree of freedom,

attributed to the ball joint connection. The buoyant legs exhibit a lower pitch natural frequency than the deck, indicating a relatively higher compliance in the pitch degree of freedom. This finding also confirms the efficacy of the ball joints in restraining rotational motion from the buoyant legs to the deck.

Based on the analysis of damping ratios, it is noted that the surge degree of freedom exhibited higher damping in both the deck and buoyant leg. Specifically, the damping in the heave and pitch directions of the deck was identified to be 9.5% and 57.3% greater, respectively, than that of the buoyant leg.

**Table 4.** Natural frequencies and damping ratios of offshore triceratops.

Parameters	Deck			Buoyant Leg		
	Surge	Heave	Pitch	Surge	Heave	Pitch
Natural frequencies (rad/s)	0.028	2.964	1.433	0.028	2.923	0.238
Damping ratio (%)	3.93	1.16	1.78	4.06	1.05	0.76

The RAOs were determined by analyzing the response of the offshore triceratops to a range of regular wave frequencies (0.1 rad/s to 1.0 rad/s) at a wave height of 4.0 m. Figure 8 depicts the deck RAOs of the offshore triceratops. Notably, within the assessed frequency range, primary peaks in surge, heave, and pitch degrees-of-freedom occurred at 0.238 rad/s, corresponding to the pitch natural frequency of the buoyant leg. Furthermore, a secondary prominent peak was observed at 0.126 rad/s in the heave and pitch degrees-of-freedom, approximating 5 times the surge natural frequency of the deck and buoyant legs.

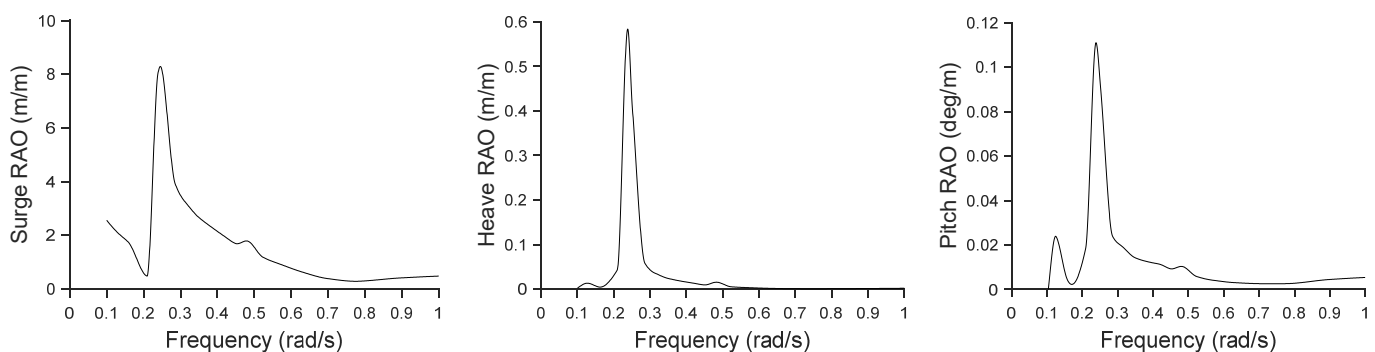


**Figure 8.** Response Amplitude Operators of the deck.

#### 4.4. Model Validation

The comparison of the natural frequencies derived in the current study with existing literature is presented in Table 5. Nagavinothini and Chandrasekaran [27] reported the dynamic response of offshore triceratops for ultradeep waters, utilizing the platform with similar geometrical and payload used in the present study. Chandrasekaran and Madhuri [44] presented the numerical and experimental investigations of offshore triceratops featuring a square deck and stiffened buoyant legs, for a water depth of 215 m. The natural surge frequency of the platform in the present study was found to be consistent with the findings in [27]. However, the heave and pitch natural frequencies of the present model were notably higher compared with the values reported in [27]. Significant discrepancies were also observed in relation to the data presented in [44]. These variations can be attributed to the modeling of the platform deck, meshing configurations, and the platform size as considered in the respective studies. Despite the deviations in the natural frequencies, the compliancy of the platform motion in the surge degree of freedom and the rigid deck motions in the heave and pitch degrees of freedom were confirmed by the lower and higher values of natural frequencies, respectively.

**Table 5.** Comparison of natural frequencies (rad/s) of offshore triceratops.

Study	Surge	Heave	Pitch
Present study	0.028	2.964	1.433
Nagavinothini and Chandrasekaran [27]	0.029	1.461	1.013
Chandrasekaran and Madhuri [44]	0.069	4.189	0.649

In addition, the response of the offshore triceratops under random wave for a moderate sea state condition, characterized by a significant wave height of 6.5 m and zero-crossing period of 8.15 s, is compared with the findings reported in the existing literature [27]. The results reveal notable differences in deck responses and tether tension, as detailed in Table 6. Specifically, the surge and heave responses exhibited variations of 12% to 17% in their maximum and minimum values. A significant reduction in the pitch response and the tether tension variation were also observed in the responses from the present model with that of the literature.

**Table 6.** Comparison of responses of offshore triceratops under moderate sea state.

Statistics	Nagavinothini and Chandrasekaran [27]				Present Study			
	Surge (m)	Heave (m)	Pitch (deg)	Tether Tension (MN)	Surge (m)	Heave (m)	Pitch (deg)	Tether Tension (MN)
Max	2.30	0.005	0.030	29.47	1.93	0.006	0.020	29.63
Min	−2.09	−0.015	−0.016	26.30	−1.80	−0.017	−0.006	27.70
Mean	0.03	−0.002	0.001	27.67	0.01	−0.007	0.001	28.71

## 5. Results and Discussion

Dynamic response analyses of offshore triceratops under random waves and freak waves were then carried out at a zero-degree wave heading angle. The developed numerical model was subjected to the random wave and freak wave (Figure 6) simulated with the wave properties listed in Table 1. This section presents the analysis of the deck, buoyant legs, and tethers. The response of the platform to random and freak waves was studied across all degrees of freedom, revealing that the sway, roll, and yaw responses of the deck and buoyant legs are negligible. Hence, the surge, heave, and pitch response of deck and buoyant legs under random and freak waves were compared through detailed statistical analysis, response time histories, and power spectral density (PSD) plots.

### 5.1. Deck Response

The surge and pitch responses of the deck exhibited periodic behavior under both random and freak waves, while the heave response was significantly influenced by the taut moored tethers. Detailed statistics of the deck responses are provided in Table 7. The analysis revealed that the occurrence of a freak wave led to a twofold increase in the absolute maximum deck surge response compared with that under random waves. Additionally, a slight mean shift towards the negative surge direction and a 14.55% increase in standard deviation were noted due to the impact of the freak wave. In the heave degree of freedom, a substantial increase in the negative heave direction was observed, resulting in almost a fourfold rise in the deck heave response. Additionally, notable variations were observed in both positive and negative pitch directions, with the absolute maximum pitch response exhibiting a 40% increase under the influence of the freak wave. It is noteworthy that the mean shift and standard deviation variations induced by the freak wave in the heave and pitch responses were comparatively smaller than those in the surge response.

The time series response and PSD plots in the surge, heave, and pitch degrees of freedom are shown in Figure 9. Notably, in the surge degree of freedom, the deck exhibited maximum and minimum responses during the occurrence of a freak wave at 592.2 s and 596.5 s, respectively, within the PW and FW time intervals. Furthermore, within the FW zone, a second maximum peak with a magnitude of 1.50 m was observed at 600.8 s.

Similarly, the minimum heave response under the influence of a freak wave was observed at 596.5 s, mirroring the surge response. Analysis of the deck pitch response revealed the occurrence of two positive peak responses at 595.6 s and 600.6 s within the PW and FW zones, respectively. Additionally, the minimum pitch response coincided with the surge and heave responses, being observed at 596.5 s, with a secondary minimum at 608.5 s in the NW zone.

**Table 7.** Statistical analysis of deck response under random and freak waves.

Response	Wave	Max	Min	Mean	Std
Surge (m)	Random	1.743	−1.584	−0.004	0.464
	Freak	2.262	−3.424	−0.003	0.543
Heave (m)	Random	0.001	−0.011	−0.001	0.001
	Freak	0.001	−0.044	−0.001	0.002
Pitch (deg)	Random	0.015	−0.007	0.001	0.002
	Freak	0.025	−0.016	0.001	0.003

In the surge PSD, the primary peak appears at the wave frequency of 0.59 rad/s under both random and freak waves. Notably, the magnitude of the peak resulting from the freak wave action ( $5.35 \text{ m}^2 \text{ s}$ ) was found to be 1.97 times higher than that observed under random wave action. Significant peaks were also observed near the surge natural frequency (0.028 rad/s) and the pitch natural frequency of the buoyant leg (0.238 rad/s), with the magnitude under freak wave being 1.67 and 1.96 times larger than that induced by random waves, respectively.

From the PSD analysis of the deck in heave degree of freedom, multiple peaks were detected in both wave scenarios and the response to freak waves exhibited greater amplitudes across all the observed peaks. The primary peak occurred at a frequency of 0.005 rad/s, with the magnitude under freak wave conditions being 5.5 times larger than that under random waves. Particularly, substantial peaks in the heave PSD were noted at lower frequencies, below 0.20 rad/s, and the patterns observed in the PSD under random and freak wave conditions were found to be consistent. Additionally, a dominant peak in the heave PSD at higher frequencies was identified at approximately 1.22 rad/s, which is approximately twice the wave frequency. It is also important to note that the peaks near the wave frequency and natural frequencies were absent in the heave PSD of the deck, possibly due to the intricate interaction between the deck and the buoyant legs.

From the pitch PSD result, the dominant peaks were observed at the frequencies of 0.005 rad/s and 1.22 rad/s, similar to the heave response suggesting a correlation between heave and pitch movements of the deck. Peaks with significantly larger magnitudes were also observed close to the wave frequency of 0.59 s in addition to the low-frequency peaks. The lower frequency motions in the pitch domain may be attributed to the surge-pitch coupling effect, a common occurrence in floating structures.

In order to further emphasize the effect of the freak waves, the probability of exceedance of absolute deck responses under random and freak waves is illustrated in Figure 10. As the offshore triceratops responses are inherently stochastic, comparing the probability of deck motion exceedances in different degrees of freedom clearly demonstrates the extent of the freak wave effect on the platform [45–48]. The comparison indicates that, up to a certain threshold, the probability of deck exceedance under random and freak waves was similar. However, beyond this threshold, the deck responses under freak waves showed an increasing trend. This reaffirms that freak wave action not only amplifies deck motion during the occurrence of the wave (close to  $t_c$ ) but also increases the deck motion beyond  $t_c$  in various degrees of freedom. The maximum deck responses under random waves (1.74 m surge, 0.01 m heave, and 0.015 degrees pitch) exhibit a probability of exceedance of 0.0001. Correspondingly, the probability of exceedance for the same responses under freak waves was determined to be 0.007, 0.008, and 0.004 in the surge, heave, and

pitch degrees of freedom, respectively. This reiterates the magnification effect induced by the presence of freak waves on the deck response.

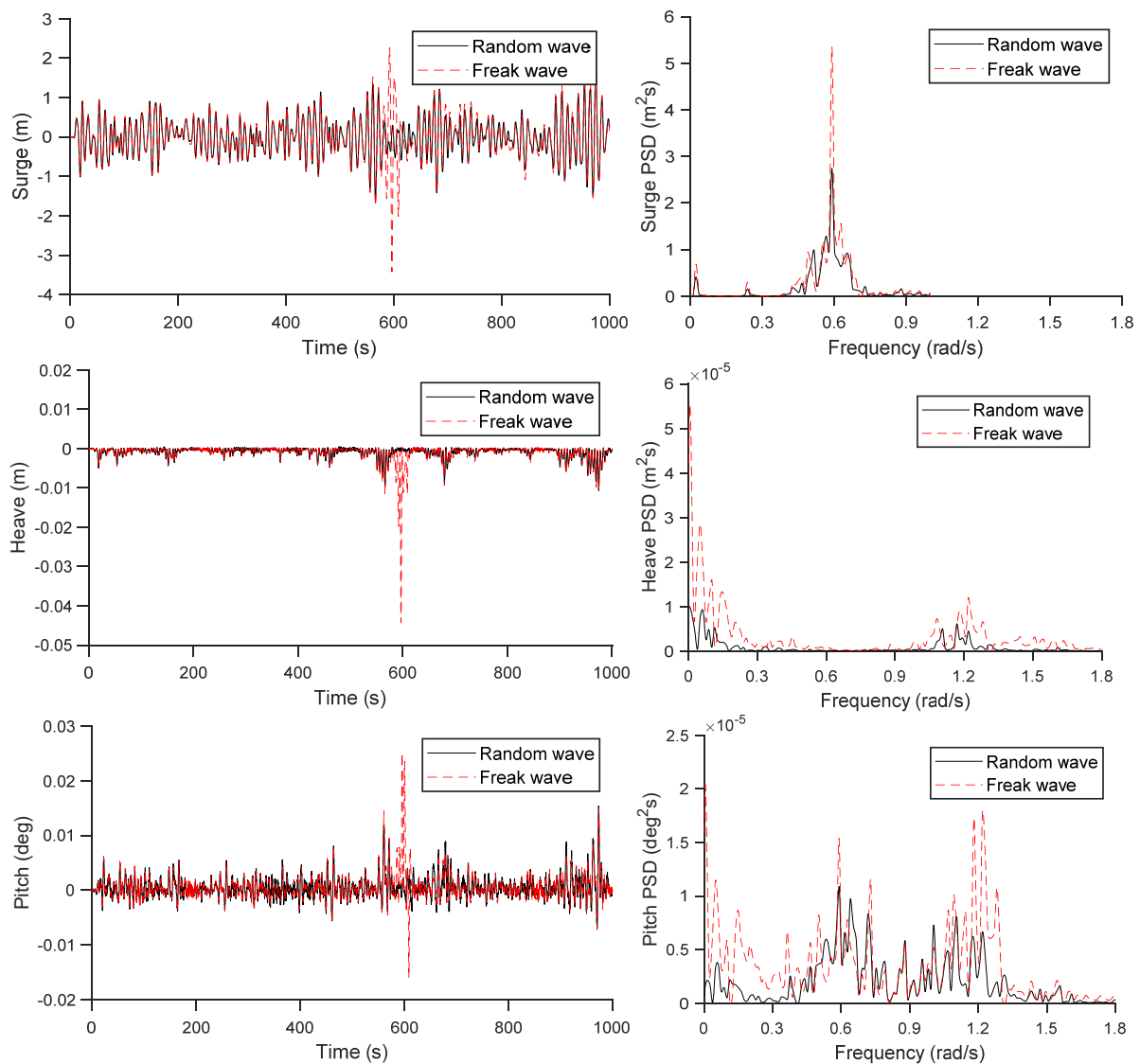


Figure 9. Deck response under random and freak waves.

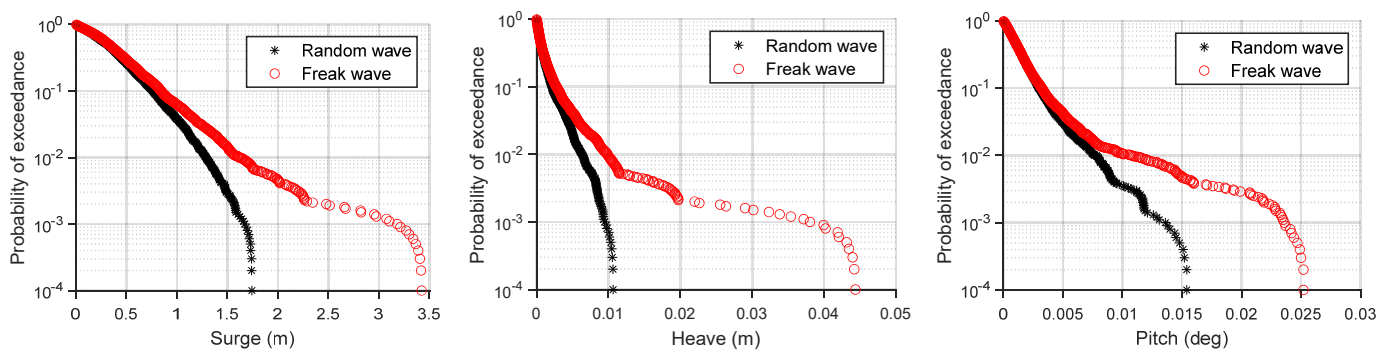
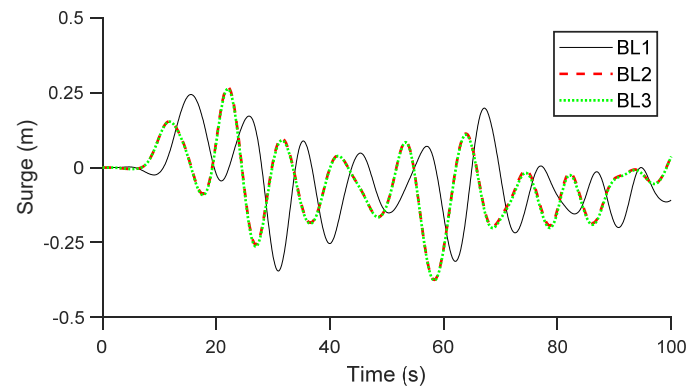


Figure 10. Comparison of probability of exceedance of deck response.

### 5.2. Buoyant Legs Response

At a zero-degree wave heading angle, the buoyant leg 1 (BL1) is positioned on the far side and the buoyant legs 2 and 3 (BL2 and BL3) are located on the near side of the wave approach (as depicted in Figure 5). BL2 and BL3 experience the impact of the freak wave before BL1, resulting in a complex interaction between the platform deck and the buoyant legs. This variance in the timing of the freak wave action on the buoyant legs introduces a delay in the maximum responses on the platform relative to the occurrence of the freak wave. This phase lag can be evidently seen from the surge responses of the buoyant legs under freak waves, shown in Figure 11.



**Figure 11.** Surge response of buoyant legs under freak waves.

Figure 12 illustrates the varying absolute maximum response amplitudes of all three buoyant legs across different degrees of freedom. Notably, it is evident that the responses of BL2 and BL3 are closely aligned due to their positions in relation to the wave approach angle. Additionally, the surge and pitch responses of BL1 were found to exceed those of BL2 and BL3. In the heave degree of freedom, the most prominent response was observed in BL2 under both wave scenarios. It was observed that the impact of a freak wave was notably greater in the case of BL2 in the surge, heave, and pitch responses, with an increase of approximately 33.38%, 73.33%, and 43.67% compared with the responses under random wave conditions, respectively.

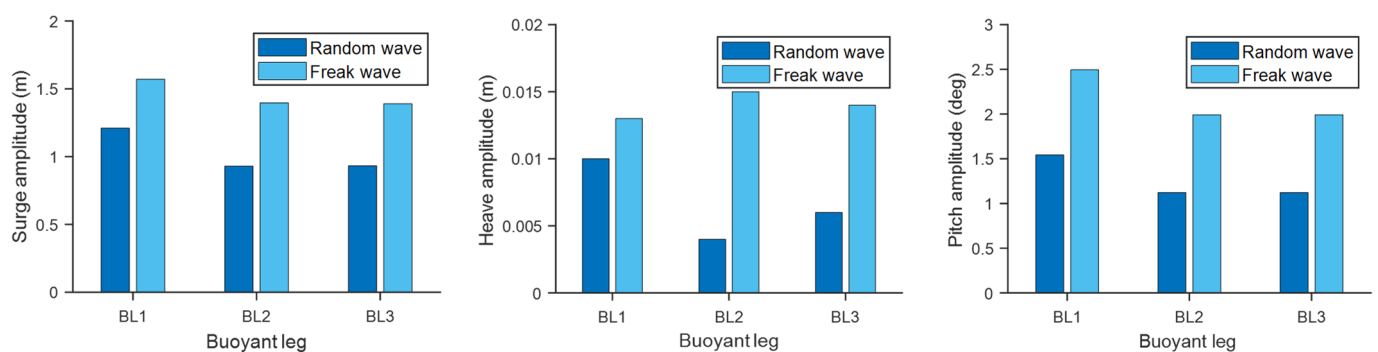


**Figure 12.** Comparison of buoyant legs response under random and freak waves.

The statistical analysis results of the buoyant legs' response under random and freak waves are detailed in Table 8. The response time histories and PSD of BL1 are shown in Figure 13. The absolute maximum surge response under freak waves occurred in the negative surge direction. The peak values were detected at 609.5 s in the NW zone in BL1 and 596.2 s in the FW zone in BL2 and BL3. This demonstrates a phase shift in the surge response of buoyant legs BL2 and BL3 in comparison to BL1, in the direction of wave approach. This phenomenon contributes to the intricate behavior of the offshore structure, with maximum and minimum responses occurring away from the FW zone. Also, the freak

wave induced a significant variation in the response pattern of the buoyant legs following the occurrence of the peak at 600 s, as depicted in the surge response time history of BL1 in Figure 13. Furthermore, the maximum surge response was observed at 687.8 s and 973.8 s away from the FW zone in BL1 and BL2, respectively. This underscores the prolonged effect of the freak wave on the platform.

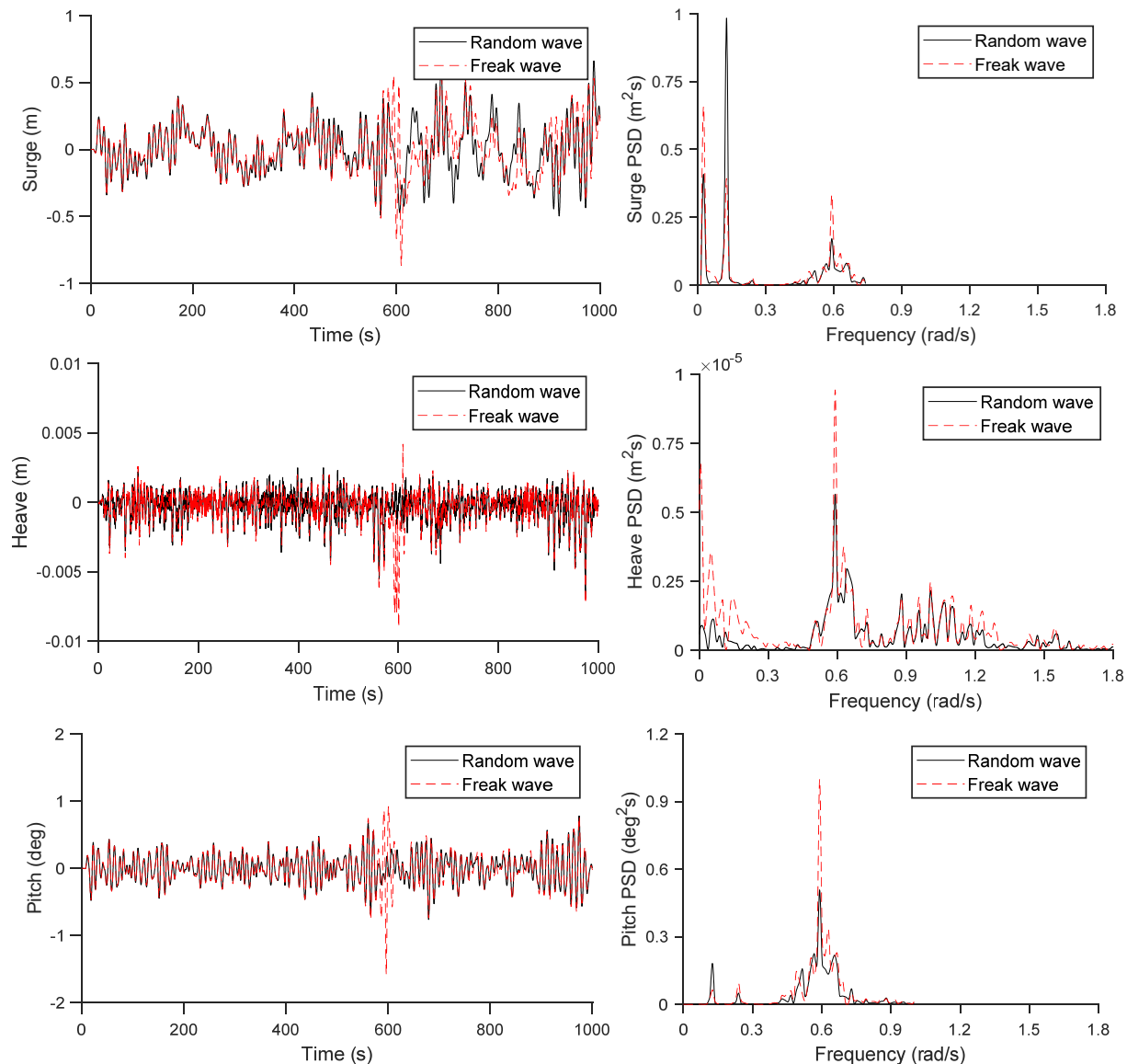


**Figure 13.** BL1 response under random and freak waves.

In the heave response of BL1, the negative peaks were recorded at 600.6 s, 596.3 s, and 593 s, whereas a positive peak was observed at 609 s. Similarly, in the heave response of BL2, positive and negative peaks were observed at 596.5 s and 598.9 s, respectively; an identical response was observed in BL3. The heave response of buoyant legs exhibited peaks at time durations similar to those seen in the pitch response of the deck, indicating clear coupling between the heave and pitch degrees of freedom despite the presence of the ball joint restraint. This coupling leads to a slight increase in the pitch response of the deck, however, with a magnitude significantly lower than that of the pitch response in buoyant legs. In the pitch response of BL1, the absolute maximum occurred at 596.4 s in the FW zone in the negative direction, while positive peaks were observed at 591.8 s and 600.8 s in the PW and FW zones. Analogous to the deck response, the surge and pitch responses

of buoyant legs exhibited a slight mean shift and increased standard deviation due to the impact of a freak wave.

In the surge PSD of BL1, the first peak occurs at the surge natural frequency where the freak wave action maximizes the peak magnitude by 37%. The next peak was observed at 0.126 rad/s, equal to five times the surge's natural frequency. At this peak, the PSD magnitude associated with the surge response to the freak wave is 2.5 times less than that of the random wave. Another significant peak is observed at the wave frequency, where the freak wave effect was found to be dominant. In the heave direction, a prominent peak is found in close proximity to the wave frequency, exhibiting a 1.70 times larger response magnitude under the freak wave. The heave PSD of buoyant legs also portrays substantial peaks in the lower frequency range of 0–0.12 rad/s, indicating coupling between surge and heave degrees of freedom. Notably, under the influence of freak waves, these peaks shift towards larger frequency zones. Furthermore, multiple peaks are observed in the frequency range of 0.8–1.3 rad/s, similar to the pitch PSD of the deck, confirming the coupling between heave and pitch degrees of freedom in the buoyant leg and deck, respectively.

In pitch degree of freedom, the dominant peak in PSD was observed at the wave frequency, indicating a 1.8 times dominance of freak wave action. Additionally, a second significant peak was identified at 0.239 rad/s, near the pitch natural frequency of the buoyant leg. The third peak at the frequency of 0.123 rad/s, which is five times the surge's natural frequency, showcased a 55% reduction in magnitude under freak wave conditions compared with random waves. These findings underscore the influence of wave frequency and the pitch natural frequency of the buoyant leg. Moreover, the occurrence of dominant peaks highlighted the coupling between various degrees of freedom.

**Table 8.** Statistical analysis of buoyant leg response under random and freak waves.

Buoyant Leg	Response	Wave	Max	Min	Mean	Std
BL1	Surge (m)	Random	0.713	−0.497	0.004	0.187
		Freak	0.706	−0.864	0.005	0.190
	Heave (m)	Random	0.003	−0.007	0	0.001
		Freak	0.004	−0.009	0	0.001
	Pitch (deg)	Random	0.779	−0.764	−0.004	0.208
		Freak	0.917	−1.578	−0.003	0.238
BL2	Surge (m)	Random	0.504	−0.426	−0.009	0.148
		Freak	0.547	−0.849	−0.011	0.170
	Heave (m)	Random	0.001	−0.003	0	0.001
		Freak	0.002	−0.013	0	0.001
	Pitch (deg)	Random	0.550	−0.572	0.003	0.162
		Freak	0.867	−1.125	0.005	0.189
BL3	Surge (m)	Random	0.500	−0.432	−0.013	0.148
		Freak	0.541	−0.849	−0.015	0.169
	Heave (m)	Random	0.002	−0.004	0	0.001
		Freak	0.002	−0.012	0	0.001
	Pitch (deg)	Random	0.550	−0.572	0.003	0.162
		Freak	0.866	−1.126	0.004	0.189

### 5.3. Tether Response

Since the platform is connected to the seabed by taut moored tethers with initial pretension, the wave action results in the tether tension variation leading to tightening and slackening of the tethers. For a compliant platform like offshore triceratops, the assessment of tether tension variation under extreme environmental conditions is crucial as it affects the functionality and station keeping of the platform. The comparison of the total tether tension variation under random and freak waves is shown in Figure 14. Similar to the

buoyant leg responses, the tension variation in the tethers connecting BL2 and BL3 showed close similarities. It was observed that the freak magnification of tension was higher in the tether of BL1 compared with the other tethers.

The variation in tether tension within all three buoyant legs was carefully examined, and the corresponding statistical analysis findings are detailed in Table 9. It was noted that the occurrence of freak waves led to a 2.6-fold increase in tether tension. Additionally, a noticeable shift from the initial pretension was observed, particularly pronounced in the case of BL1. Furthermore, analogous to the responses observed in the deck and buoyant legs, the effect of these extreme waves resulted in an increase in the standard deviation of tether tension.

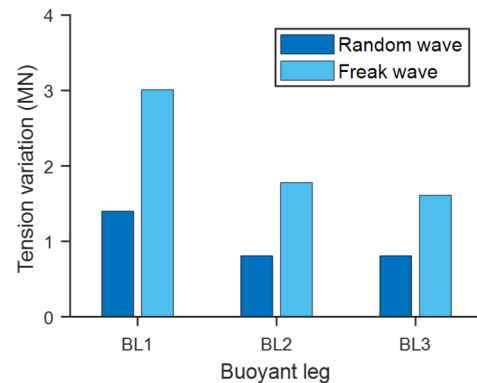


**Figure 14.** Comparison of tether tension variation.

**Table 9.** Statistical analysis of tether tension (MN) under random and freak waves.

Buoyant Leg	Wave	Max	Min	Mean	Std
BL1	Random	0.700	−0.700	−0.072	2.038
	Freak	1.830	−1.180	−0.083	0.231
BL2	Random	0.430	−0.377	−0.022	1.152
	Freak	0.647	−1.130	−0.002	0.125
BL3	Random	0.430	−0.377	−0.022	1.134
	Freak	0.590	−1.020	−0.002	0.126

In order to provide a clear understanding of the impact of freak waves, the variation in tether tension was depicted by establishing the initial pretension of the tether as the zero-mean value in Figure 15. The occurrence of maximum and minimum tether tension under freak waves was noted at 596.4 s and 593.4 s, respectively, within the FW zone. Additionally, a second maximum peak was identified at 608.8 s within the NW zone. The timing of peak tether tension responses closely mirrored the peak heave response in the buoyant legs. The tether tension PSD, as depicted in Figure 15, revealed a dominant peak at the wave frequency under both random and freak waves. Furthermore, the PSD magnitude under the freak wave was nearly twice as large as that associated with random waves. Notable peaks in the frequency range of 0.8–1.2 rad/s were also observed in the PSD plot, similar to the response of the buoyant legs in heave degree of freedom. Despite a similar tether tension PSD pattern under both scenarios, the magnitude under freak wave was consistently higher across all observed peaks.

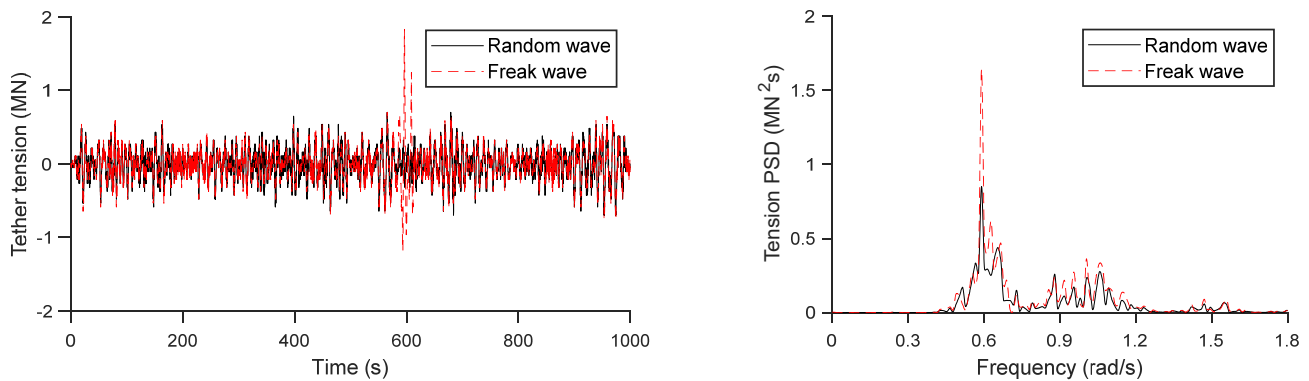


**Figure 15.** Tether tension variation under random and freak waves.

#### 5.4. Effect of Ball Joints

One of the main advantages of offshore triceratops that can extend their operability to ultradeep waters is the presence of ball joints, which restrain the rotational motion from the buoyant legs to the deck. To evaluate the effectiveness of the ball joints, the comparison of the absolute maximum pitch responses of the deck and buoyant legs under random and freak waves is presented in Figure 16. The results demonstrate that the pitch response of the deck is minimal compared with that of the buoyant legs under both wave action scenarios. Even when subjected to a freak wave, which generally amplifies platform responses to all degrees of freedom, the maximum pitch response of the deck is only 0.025 degrees—a value 63 times smaller than the maximum pitch response of BL1 (2.524 degrees). Notably, the maximum pitch response of the deck under a freak wave is even smaller than the maximum pitch response of BL1 under a random wave (0.779 degrees). This underscores the effectiveness of the ball joints in attenuating the deck's rotational motion, even in extreme environmental conditions.

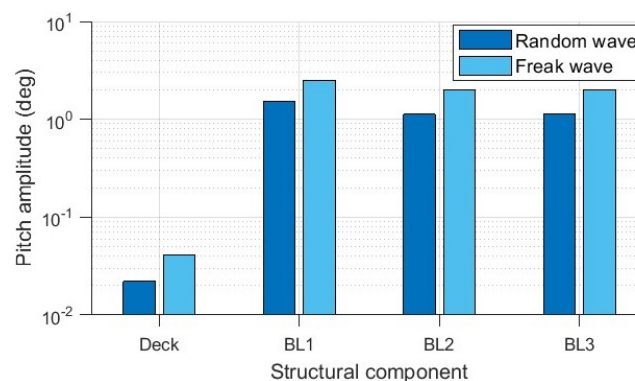


**Figure 16.** Pitch response under random and freak waves.

## 6. Conclusions

The primary objective of the current study is to explore the impact of freak waves on offshore triceratops in ultradeep waters. The numerical model of the platform, created using ANSYS AQWA, was exposed to two types of waves: (i) a random wave, and (ii) a freak wave simulated using the dual superposition model. The waves were generated based on the JONSWAP spectrum with a significant wave height of 6 m and a peak period of 10 s. The crest amplitude of the simulated freak wave was 13.45 m, approximately 2.3 times greater than the random wave height. The findings indicated that the freak wave significantly influenced the response of the platform in all degrees of freedom. Furthermore, statistical analysis revealed substantial variations in response patterns under freak wave conditions compared with random waves.

The deck surge and heave responses of the platform revealed a twofold and fourfold increase in the absolute maximum responses compared with those of random waves. The PSD analysis of the deck indicated coupling among the surge, heave, and pitch degrees of freedom. Large magnitude peaks close to the wave frequency were observed in surge and pitch responses, where the peak magnitude from freak wave action was found to be 1.97 and 1.37 times larger than that observed under random wave action. The positioning of the buoyant legs relative to the wave approach angle significantly impacted the timing and magnitude of their responses. Phase shifts, peak variations, and coupling effects between different degrees of freedom were observed, emphasizing the complexity of the platform's response to freak wave conditions. The impact of a freak wave was notably greater in the case of BL2 in the surge, heave, and pitch responses, with an increase of approximately 33.38%, 73.33%, and 43.67% compared with the responses under random wave conditions. The comparison of total tether tension variation under random and freak waves, as well as the statistical analysis findings, indicates a 2.6-fold increase in tether tension due to the occurrence of freak waves. Additionally, there was a noticeable shift from the initial pretension, particularly pronounced in the case of BL1. The timing of the peak tether tension responses closely mirrored the peak heave response in the buoyant legs.

In conclusion, this study highlighted the intricate behavior of an offshore structure in response to both random and freak waves. The findings provide valuable insights into the pronounced effects of freak waves on tether tension, which can inform crucial design and operational considerations for similar offshore structures. Overall, this study provides valuable insights into the behavior of offshore structures under the influence of freak waves, emphasizing the significance of comprehending and mitigating the potential consequences of such exceptional events. The results will benefit offshore engineers and academic researchers in their pursuit to improve the safety of offshore platforms against freak wave conditions.

This study represents an initial effort to explore the impact of extreme waves on offshore triceratops in ultradeep water. The future research direction includes a detailed parametric analysis of the hydrodynamic response of offshore triceratops, encompassing factors such as focusing location, crest amplitude, wave period, large crest, and deep trough associated with extreme waves.

**Author Contributions:** Conceptualization, N.R. and B.B.; methodology, N.R.; software, N.R.; validation, N.R. and B.B.; formal analysis, N.R.; investigation, N.R.; resources, N.R.; data curation, N.R.; writing—original draft preparation, N.R.; writing—review and editing, N.R. and B.B.; visualization, N.R. and B.B.; supervision, B.B. All authors have read and agreed to the published version of the manuscript.

**Funding:** This research is supported by the Ratchadapisek Somphot Fund for Postdoctoral Fellowship, Chulalongkorn University.

**Institutional Review Board Statement:** Not applicable.

**Informed Consent Statement:** Not applicable.

**Data Availability Statement:** Data availability is based on request.

**Conflicts of Interest:** The authors declare no conflicts of interest.

## References

1. Xue, S.; Xu, G.; Xie, W.; Xu, L.; Jiang, Z. Characteristics of freak wave and its interaction with marine structures: A review. *Ocean Eng.* **2023**, *287*, 115764. [\[CrossRef\]](#)
2. Ji, X.; Li, A.; Li, J.; Wang, L.; Wang, D. Research on the statistical characteristic of freak waves based on observed wave data. *Ocean Eng.* **2022**, *243*, 110323. [\[CrossRef\]](#)
3. Zhang, H.; Tang, W.; Yuan, Y.; Xue, H.; Qin, H. The three-dimensional green-water event study on a fixed simplified wall-sided ship under freak waves. *Ocean Eng.* **2022**, *251*, 111096. [\[CrossRef\]](#)
4. Cui, C.; Pan, W.B. Experimental Study on the Wavelengths of Two-Dimensional and Three-Dimensional Freak Waves. *China Ocean Eng.* **2023**, *37*, 154–164. [\[CrossRef\]](#)

5. Draper, L. 'FREAK' OCEAN WAVES. *Weather* **1966**, *21*, 2–4. [[CrossRef](#)]
6. Clauss, G.F. Dramas of the sea: Episodic waves and their impact on offshore structures. *Appl. Ocean Res.* **2002**, *24*, 147–161. [[CrossRef](#)]
7. Dysthe, K.; Krogstad, H.E.; Müller, P. Oceanic rogue waves. *Annu. Rev. Fluid Mech.* **2008**, *40*, 287–310. [[CrossRef](#)]
8. Rosenthal, W.; Lehner, S. Rogue waves: Results of the MaxWave project. *J. Offshore Mech. Arct. Eng.* **2008**, *130*, 021006. [[CrossRef](#)]
9. Soares, C.G.; Cherneva, Z.; Antao, E.M. Characteristics of abnormal waves in North Sea storm sea states. *Appl. Ocean Res.* **2003**, *25*, 337–344. [[CrossRef](#)]
10. Pleskachevsky, A.L.; Lehner, S.; Rosenthal, W. Storm observations by remote sensing and influences of gustiness on ocean waves and on generation of rogue waves. *Ocean Dyn.* **2012**, *62*, 1335–1351. [[CrossRef](#)]
11. Hu, Z.; Tang, W.; Xue, H. A probability-based superposition model of freak wave simulation. *Appl. Ocean Res.* **2014**, *47*, 284–290. [[CrossRef](#)]
12. Pan, W.; He, M.; Cui, C. Experimental Study on Hydrodynamic Characteristics of a Submerged Floating Tunnel under Freak Waves (I: Time-Domain Study). *J. Mar. Sci. Eng.* **2023**, *11*, 977. [[CrossRef](#)]
13. Xu, P.; Zhang, Z.; Li, S.; Song, Q.; Liu, W. Numerical Investigation into the Dynamic Responses of Floating Photovoltaic Platform and Mooring Line Structures under Freak Waves. *J. Mar. Sci. Eng.* **2024**, *12*, 96. [[CrossRef](#)]
14. Li, Y.; Li, H.; Wang, Z.; Li, Y.; Wang, B.; Tang, Y. The dynamic response of a Spar-type floating wind turbine under freak waves with different properties. *Mar. Struct.* **2023**, *91*, 103471. [[CrossRef](#)]
15. Zeng, F.; Zhang, N.; Huang, G.; Gu, Q.; He, M. Experimental study on dynamic response of a floating offshore wind turbine under various freak wave profiles. *Mar. Struct.* **2023**, *88*, 103362. [[CrossRef](#)]
16. Zhong, W.; Zhang, X.; Wan, D. Hydrodynamic characteristics of a 15 MW semi-submersible floating offshore wind turbine in freak waves. *Ocean Eng.* **2023**, *283*, 115094. [[CrossRef](#)]
17. Zeng, F.; Zhang, N.; Huang, G.; Gu, Q.; He, M. Dynamic response of floating offshore wind turbines under freak waves with large crest and deep trough. *Energy* **2023**, *278*, 127679. [[CrossRef](#)]
18. Huo, F.; Zhao, Y.; Zhang, J.; Zhang, M.; Yuan, Z.M. Study on wave slamming characteristics of a typical floating wind turbine under freak waves. *Ocean Eng.* **2023**, *269*, 113464. [[CrossRef](#)]
19. Huo, F.; Yang, H.; Yao, Z.; An, K.; Xu, S. Study on slamming pressure characteristics of platform under freak wave. *J. Mar. Sci. Eng.* **2021**, *9*, 1266. [[CrossRef](#)]
20. Luo, M.; Koh, C.G.; Lee, W.X.; Lin, P.; Reeve, D.E. Experimental study of freak wave impacts on a tension-leg platform. *Mar. Struct.* **2020**, *74*, 102821. [[CrossRef](#)]
21. Tang, Y.G.; Li, Y.; Wang, B.; Liu, S.X.; Zhu, L.H. Dynamic analysis of turret-moored FPSO system in freak wave. *China Ocean Eng.* **2016**, *30*, 521–534. [[CrossRef](#)]
22. Gao, J.; Mi, C.; Song, Z.; Liu, Y. Transient gap resonance between two closely-spaced boxes triggered by nonlinear focused wave groups. *Ocean Eng.* **2024**, *305*, 117938. [[CrossRef](#)]
23. Gao, J.; Ma, X.; Zang, J.; Dong, G.; Ma, X.; Zhu, Y.; Zhou, L. Numerical investigation of harbor oscillations induced by focused transient wave groups. *Coast. Eng.* **2020**, *158*, 103670. [[CrossRef](#)]
24. Gao, J.; Chen, H.; Zang, J.; Chen, L.; Wang, G.; Zhu, Y. Numerical investigations of gap resonance excited by focused transient wave groups. *Ocean Eng.* **2020**, *212*, 107628. [[CrossRef](#)]
25. Gao, J.; Lyu, J.; Wang, J.-H.; Zhang, J.; Liu, Q.; Zang, J.; Zou, T. Study on transient gap resonance with consideration of the motion of floating body. *China Ocean Eng.* **2022**, *36*, 994–1006. [[CrossRef](#)]
26. Chandrasekaran, S.; Nagavinothini, R. Dynamic analyses and preliminary design of offshore triceratops in ultra-deep waters. *Innov. Infrastruct. Solut.* **2018**, *3*, 16. [[CrossRef](#)]
27. Nagavinothini, R.; Chandrasekaran, S. Dynamic analyses of offshore triceratops in ultra-deep waters under wind, wave, and current. *Structures* **2019**, *20*, 279–289. [[CrossRef](#)]
28. Chandrasekaran, S.; Nagavinothini, R. Tether analyses of offshore triceratops under wind, wave, and current. *Mar. Syst. Ocean Technol.* **2018**, *13*, 34–42. [[CrossRef](#)]
29. Srinivasan, C.; Nagavinothini, R. ICE-INDUCED response of offshore triceratops. *Ocean Eng.* **2019**, *180*, 71–96. [[CrossRef](#)]
30. Chandrasekaran, S.; Nagavinothini, R. Tether analyses of offshore triceratops under ice force due to continuous crushing. *Innov. Infrastruct. Solut.* **2019**, *4*, 25. [[CrossRef](#)]
31. Chandrasekaran, S.; Nannaware, M. Response analyses of offshore triceratops to seismic activities. *Ships Offshore Struct.* **2014**, *9*, 633–642. [[CrossRef](#)]
32. Chandrasekaran, S.; Nagavinothini, R. Offshore Triceratops Under Impact Forces in Ultra Deep Arctic Waters. *Int. J. Steel Struct.* **2020**, *20*, 464–479. [[CrossRef](#)]
33. Chandrasekaran, S.; Ravichandran, N. Parametric studies on the impact response of offshore triceratops in ultra-deep waters. *Struct. Infrastruct. Eng.* **2020**, *16*, 1002–1018. [[CrossRef](#)]
34. Orzech, M.D.; Wang, D. Measured rogue waves and their environment. *J. Mar. Sci. Eng.* **2020**, *8*, 890. [[CrossRef](#)]
35. Wu, G.; Han, L.; Zhang, L. Numerical Simulation and Backscattering Characteristics of Freak Waves Based on JONSWAP Spectrum. *Front. Mar. Sci.* **2022**, *9*, 868737. [[CrossRef](#)]
36. Klinting, P.; Sand, S.E. Analysis of Prototype Freak Waves. 1987. Available online: <https://api.semanticscholar.org/CorpusID:128156070> (accessed on 31 May 2024).

37. Longuet-Higgins, M.S. On the Statistical Distribution of the Heights of Sea Waves. *J. Mar. Res.* **1952**, *11*, 245–266.
38. Kriebel, D.L.; Alsina, M.V. Simulation of extreme waves in a background random sea. In Proceedings of the International Offshore and Polar Engineering Conference, Seattle, WA, USA, 28 May–2 June 2000.
39. Hasselmann, K.; Barnett, T.P.; Bouws, E.; Carlson, H.; Cartwright, D.E.; Enke, K.; Ewing, J.A.; Gienapp, A.; Hasselmann, D.E.; Kruseman, P.; et al. Measurements of wind-wave growth and swell decay during the joint North Sea wave project (JONSWAP). *Ergänzung zur Deut. Hydrogr. Z. Reihe A* **1973**, *12*, 1–95.
40. Onorato, M.; Osborne, A.R.; Serio, M.; Bertone, S. Freak waves in random oceanic sea states. *Phys. Rev. Lett.* **2001**, *86*, 5831–5834. [[CrossRef](#)] [[PubMed](#)]
41. Komen, G.J.; Cavaleri, L.; A Donelan, M.; Hasselmann, K.; Hasselmann, S.; Janssen, P.A.E.M. *Dynamics and Modelling of Ocean waves*; Cambridge University Press: Cambridge, UK, 1996. [[CrossRef](#)]
42. White, C.N.; Copple, R.W.; Capanoglu, C. Triceratops: An effective platform for developing oil and gas fields in deep and ultra-deep water. In Proceedings of the International Offshore and Polar Engineering Conference, Seoul, Republic of Korea, 19–24 June 2005.
43. Chen, Y.; Zimmer, R.A.; De Oliveira, J.G.; Jan, H.Y. Buckling and ultimate strength of stiffened cylinders: Model experiments and strength formulations. In Proceedings of the Annual Offshore Technology Conference, Houston, TX, USA, 6–9 May 1985. [[CrossRef](#)]
44. Chandrasekaran, S.; Madhuri, S. Dynamic response of offshore triceratops: Numerical and experimental investigations. *Ocean Eng.* **2015**, *109*, 401–409. [[CrossRef](#)]
45. Pegalajar-Jurado, A.; Hansen, A.M.; Laugesen, R.; Mikkelsen, R.F.; Borg, M.; Kim, T.; Heilskov, N.F.; Bredmose, H. Experimental and numerical study of a 10MW TLP wind turbine in waves and wind. *J. Phys. Conf. Ser.* **2016**, *753*, 092007. [[CrossRef](#)]
46. Hansen, C.L.; Bredmose, H.; Vincent, M.; Steffensen, S.E.; Pegalajar-Jurado, A.; Jensen, B.; Diken, M. Resonant response of a flexible semi-submersible floating structure: Experimental analysis and second-order modelling. *J. Fluid Mech.* **2024**, *982*, A7. [[CrossRef](#)]
47. Diep Nguyen, T.T.; Nguyen, V.M.; Yoon, H.K. Experimental and numerical simulation on dynamics of a moored semi-submersible in various wave directions. *Sci. Prog.* **2021**, *104*, 1–29. [[CrossRef](#)] [[PubMed](#)]
48. ITTC-Recommended Practices and Guidelines: Sloshing Model Tests, Seakeeping Committee of 28th International Towing Tank Conference. 2017. Available online: <https://www.ittc.info/media/8111/75-02-07-027.pdf> (accessed on 8 July 2024).

**Disclaimer/Publisher’s Note:** The statements, opinions and data contained in all publications are solely those of the individual author(s) and contributor(s) and not of MDPI and/or the editor(s). MDPI and/or the editor(s) disclaim responsibility for any injury to people or property resulting from any ideas, methods, instructions or products referred to in the content.